JOURNAL OF COMPUTATIONAL PHYSICS 36, 1–19 (1980)

Plasma Self-Heating and Saturation due to Numerical Instabilities*

CHARLES K. BIRDSALL† AND NEIL MARON

Lawrence Livermore Laboratory, University of California, Livermore, California 94550

Received February 12, 1978; revised May 22, 1979

The cold-beam nonphysical instability due to the aliases produced by the numerical spatial grid is presented in detail for momentum-conserving linear weighting codes. Additions to previous work include: linear analysis dispersion diagrams showing large growth rates, $\omega_i \leqslant 0.2\,\omega_p$; methods for reducing ω_i, effectively broadening the finite-size particle width; simulation results verifying the linear theory, plus plots showing the $p = 1$ alias in phase space (v_x, x); the growth of beam thermal spread (v_t^2 in temperature) and loss of energy conservation; end-of-growth (saturation) at small thermal spread ($\lambda_D/\Delta x = v_t/\omega_p \Delta x \simeq 0.046$, for $\lambda_B/\Delta x \equiv v_0/\omega_p \Delta x \geqslant 0.3$, i.e., $v_t \leqslant 0.14 v_0$), with return to near energy conservation (stability); demonstration of no growth for a warm beam, with v_t(initial) $\geqslant$ v_t(saturation); and the mechanism of stabilization (trapping). A thermal (Maxwellian) plasma, also nonphysically unstable at small $\lambda_D/\Delta x$, is also found to approach stabilization by self-heating. The two-stream physical instability is affected by the grid, with the aliasing instability also present; the linear theory for this is presented, with guidelines for minimizing the effects of the grid.

1. INTRODUCTION

Nonphysical plasma instabilities may be generated by interaction of the charged particles with the computational spatial grid. These have been found analytically by Langdon [1] and Chen *et al.* [2], and verified in simulation by Langdon [3], Okuda [4], and Chen *et al.* [2] for both momentum- and energy-conserving programs. (The reader will find an up-to-date compact review of simulation theory in Langdon [5].) The plasmas they studied had either a Maxwellian velocity distribution with no drift (unstable in momentum-conserving programs for $\lambda_D/\Delta x \lesssim 0.3$ and stable in energy-conserving programs) or no velocity spread, but a drift, v_0, called a cold beam

* Work performed under the auspices of the U.S. Department of Energy by the Lawrence Livermore Laboratory under contract number W-7405-ENG-48. Professor Birdsall was also supported in part by the U.S. Department of Energy at the Electronics Research Laboratory, University of California, Berkeley under contract number EY-76-S-03-0034-PA128.

† Permanent address: Electrical Engineering and Computer Science Dept., University of California, Berkeley, Calif. 94720.

0021-9991/80/070001-19$02.00/0

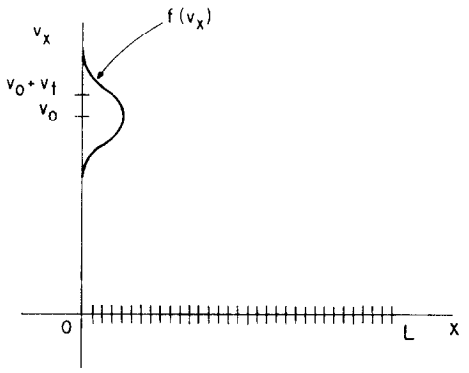

FIG. 1. One-dimensional periodic model of a beam drifting through the spatial grid used for solving for charge density, potential, and field. The drift velocity is v_0 ; the beam may be warm, with thermal velocity v_t , with distribution function as sketched. The period is L; typically the number of cells is 32, as shown.

(unstable in both programs). The temporal growth rates predicted and measured were not small (on the order of 0.1 to $0.2\omega_p$), so these nonphysical instabilities could intrude seriously on real physical effects. Indeed, adding the least amount of drift to a cold plasma (which is stable) ushers in this unwanted effect.

The model for our theory and simulations is in Fig. 1. We first explore growth rates for the cold-beam instability ($\lambda_D = 0$, $v_{\text{thermal}} = 0$), seeking various cures such as modifying the particle (and force) weightings and interlacing (two grids in one time step; see Chen *et al.* [2]), as well as by smoothing (in k space) and particle broadening. These are found to reduce growth rates by a factor of 10 to 20 (down to $0.01\omega_p$), which probably are sufficiently small to cause little trouble in most simulations.

The pertinent beam parameter here is defined by

$$B \equiv \frac{v_0}{\omega_p \Delta x} \equiv \frac{\lambda_B}{\Delta x} .$$

For all $B > 0$, momentum-conserving programs show the beam instability; for $0 < B \lesssim 1/\pi \simeq 0.3$, energy-conserving programs show the beam instability.

We next show the results of several cold-beam simulations, with momentum-conserving programs, varying B from $1/4\pi \simeq 0.08$ to 1.0. The interesting result is that the *instability heats the beam*, adding a $v_{\text{thermal}} > 0$, which increases exponentially *and then stops* at $\lambda_D/\Delta x = 0.046$ (as does the exponential growth of all other quantities): the system has become *stable*. These results were presented earlier by Birdsall *et al.* [6]. The larger the value of the beam parameter, B, the smaller the final value of v_t/v_0 . The same final value of v_t occurs, independent of the initial value of v_t , up to $(v_t)_{\text{final}}$; if $(v_t)_{\text{initial}} \gtrsim (v_t)_{\text{stable}}$, then the system is stable from the start. Hence, one may either start off with a cold beam and let the self-heating take place through to saturation or add a small velocity spread to the drift and start off stably. The theory

for saturation at $\lambda_D/\Delta x = 0.046$ has been worked out by Albritton and Nevins [7] and is given here.

A nondrifting thermal (Maxwellian) plasma was also run in the unstable region, $\lambda_D/\Delta x = 0.1$. Indeed, the plasma temperature increased rapidly at first (due to the nonphysical instability) and then more slowly (due to the larger-than-thermal field level), apparently moving toward $\lambda_D/\Delta x \simeq 0.25$ asymptotically. This is interpreted as the same form of approach to saturation as observed with the cold beam.

Finally, we show the results of linear analyses, including grid effects (the aliasing), for two opposing cold beams. The purpose is to show that the physical two-stream instability, simulated many times in many ways over the past 20 years, is little affected by the cold-beam grid instability.

2. Linear Analysis; Growth Rates

In this section, we apply the theory of Langdon [1] to a one-dimensional periodic system of period L, uniform in each period. One set of particles has drift velocity v_0; the other set, of opposite sign of charge, is immobile, simply neutralizing. There are NG cells with length $\Delta x = L/\mathrm{NG}$. The time step, Δt, is considered short so that effects of finite Δt are ignored.

All first-order perturbed quantities propagate as

$$\exp i(\omega t - kx). \tag{1}$$

Langdon's dispersion relation for one cold beam is

$$0 = \epsilon(\omega, k) = 1 - \frac{\omega_p^2}{K^2(k)} \sum_p \frac{\mathbf{k}_p \cdot \kappa(k_p)\, S^2(k_p)}{(\omega - k_p v_0)^2}, \tag{2}$$

where ω_p is the plasma frequency, K^2 is the finite-difference Laplace operator, $\kappa(k)$ is the finite-difference gradient operator, $S^2(k)$ is the Fourier transform of the effective shape of the particle, dependent on the method (order) of interpolation used, and the wave numbers are

$$k_p = k - pk_g, \qquad p = 0, \pm 1, \pm 2, \ldots, \tag{3}$$

$$k_g = \frac{2\pi}{\Delta x}. \tag{4}$$

The poles in Eq. (2) are obviously of interest and will turn out to be (roughly) the ω_{real} of the unstable modes

$$\omega_r \simeq k_p v_0 = \left(k - \frac{2\pi p}{\Delta x} v_0\right). \tag{5}$$

These frequencies are shown in Fig. 2 along with ω_{grid},

$$\omega_g = 2\pi \left(\frac{v_0}{\Delta x}\right). \tag{6}$$

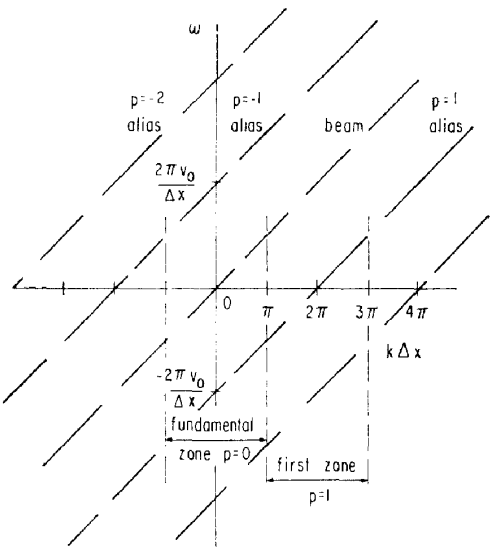

FIG. 2. Sketch of the poles of the dispersion (ω, k) relation (roughly, the location of ω_{real}) for a cold beam in a spatial grid, showing the physical pole ($p = 0$) and the alias poles ($p \neq 0$), which are due to the grid and are nonphysical.

The different spatial harmonic (Brillouin) zones are also identified. The interactions leading to instability are between the real beam and the $p = \pm 1, \pm 2$, etc., aliases; these are wholly nonphysical, a result of the (mathematical) spatial gridding.

In all of the earlier work, the drift and thermal velocities were defined in terms of a factor times $\omega_p \Delta x$; here we will be concerned with similar normalizations, with the familiar ratio of Debye length to grid spacing,

$$\frac{\lambda_D}{\Delta x} \equiv \frac{v_t}{\omega_p \Delta x} \tag{7}$$

and a similar parameter for the beam, defined by

$$B \equiv \frac{\lambda_B}{\Delta x} \equiv \frac{v_0}{\omega_p \Delta x} = \frac{1}{2\pi} \frac{\omega_g}{\omega_p}. \tag{8}$$

The nature of the instability changes in the vicinity of $\omega_p = \omega_{\text{grid}}$ such that we define *slow beams* by

$$\omega_g < \omega_p, \qquad B < 1/2\pi = 0.159 \tag{9}$$

and *fast beams* by

$$\omega_g > \omega_p, \qquad B > 1/2\pi. \tag{10}$$

Earlier simulations [1–4] were with slow beams, $B \simeq 0.12$, thus missing some important effects.

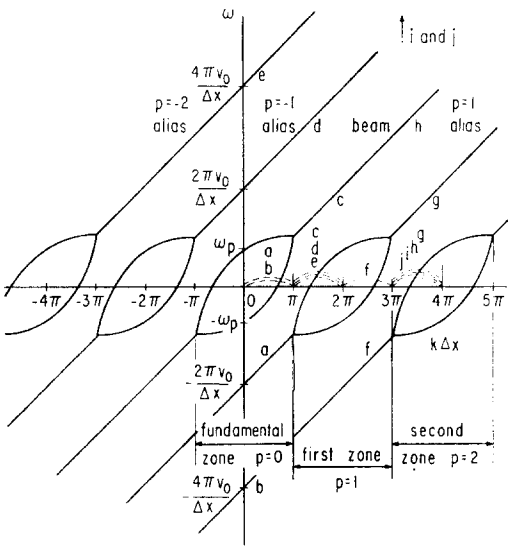

FIG. 3. Approximate solution of the dispersion relation, Eq. (2) for $B = 0.32$, $\omega_g \simeq 2\omega_p$ with $p = 0, \pm 1, \pm 2$ terms only, for real k, complex ω. ω_{real} is shown solid and ω_{imag} is shown dashed. The letters connect real and imaginary parts of ω. If more values of p were kept, there would be more ω_{imag}, but smaller than those shown.

Figure 3 shows a typical solution of Eq. (2) for a cold fast beam, $B = 0.32$ ($\simeq 1/\pi$), $\omega_g \simeq 2\omega_p$. The real parts of the roots for ω (solid lines) are much like the sketch of Fig. 2. The imaginary parts are shown dashed in Fig. 3 (and given exactly in Fig. 4); in the fundamental zone, the larger growth rate (ω_{imag}) is due to interactions between the beam and $p = 1$ alias; the smaller, between the beam and $p = 2$; those for $p > 3$ were not included in the solution but presumably would be smaller yet (nested inside $p = 2$ roots). Note that the larger growth rate, labeled a, has ω_{real} given by the $p = 1$ alias. The roots cutting through $\pm\omega_p$ at $k = 0$ are wholly real (no growth), simply the Doppler-shifted Langmuir oscillations, as smoothed by the Poisson and gradient finite-difference operators.

In solving Eq. (2), the Poisson operator, $K^2(k)$, was obtained from the usual three-point scheme so that

$$K^2(k) = k^2 \left[\frac{\sin(k\,\Delta x/2)}{(k\,\Delta x/2)}\right]^2. \tag{11}$$

The gradient operator was the usual two-point form, giving,

$$\kappa(k_p) = k_p \left[\frac{\sin(k_p\,\Delta x)}{(k_p\,\Delta x)}\right] \tag{12}$$

for momentum-conserving programs in which the particle force is an interpolation of the differenced potential, and

$$\kappa(k_p) = k_p \tag{13}$$

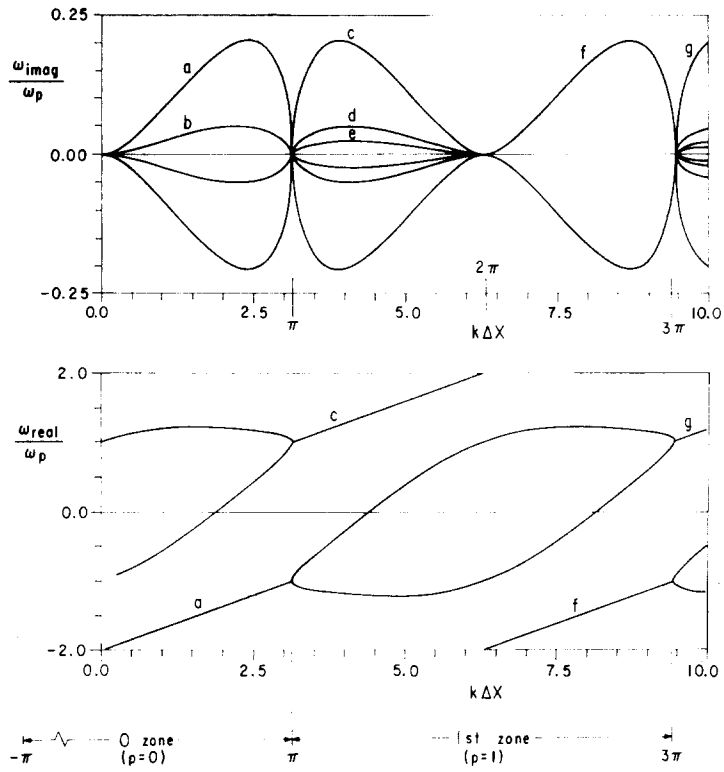

FIG. 4. Exact plots of solutions sketched in Fig. 3, for $B = 0.32$, $\omega_g \simeq 2\omega_p$.

for energy-conserving programs in which the particle force may be regarded as the derivative of the interpolated potential [5]. The shape factor transform used was

$$S(k) = \left[\frac{\sin(k\,\Delta x/2)}{(k\,\Delta x/2)}\right]^r \tag{14}$$

with $r = 2$ for linear weighting (Figs. 3 and 4, CIC and PIC) and $r = 3$ for quadratic (spline) weighting. If the transformed charge density, $\rho(k)$, is smoothed by SM(k), then SM appears outside the sum over p, as a product of ${\omega_p}^2$.

The maximum growth rate found, $(\omega_i)_{\max}$ [solving Eq. (2)], is

$$(\omega_i)_{\max} \simeq 0.2 \qquad \text{at} \qquad k\,\Delta x \simeq 3\pi/4 \tag{15}$$

meaning 11 dB growth per plasma cycle, which is uncomfortably large. This maximum value was found to be almost invariant with beam parameter, B, over the range,

$$0.08 \approx 1/4\pi \leqslant B \leqslant 4. \tag{16}$$

The character of $\omega_i(k)$ hardly changes as B increases from 0.32 (Fig. 4) to 4; however, for $B = 1/4\pi$, $1/2\pi$, $\omega_g/\omega_p = 1/2$, 1, the character change is substantial but $(\omega_i)_{\max}$ is still roughly 0.2 (Fig. 5).

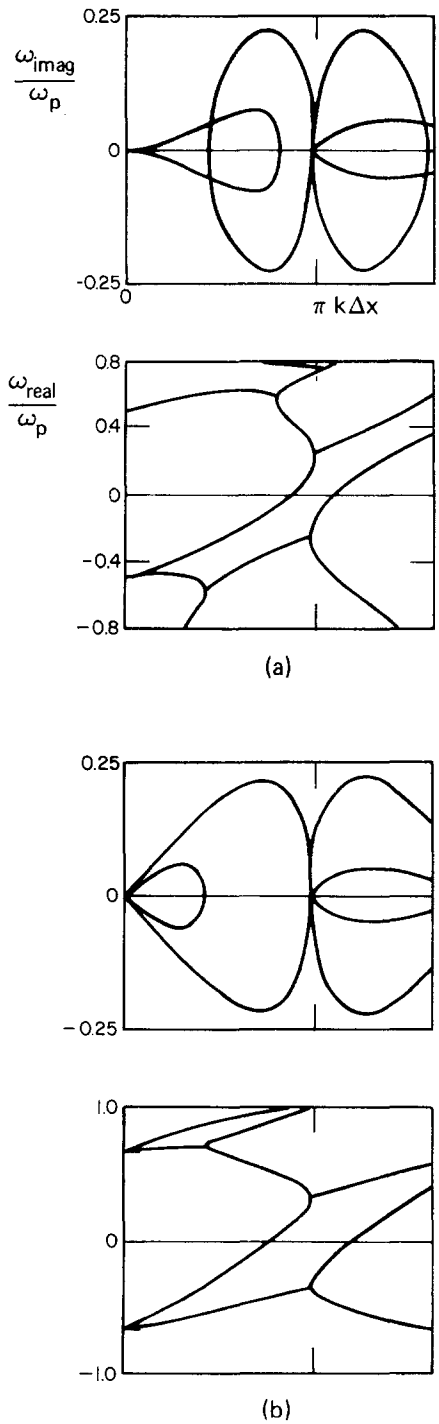

FIG. 5. Exact solutions for complex ω for (a) $B = 1/(4\pi)$ and (b) $B = 1/2\pi$ ($\omega_g/\omega_p = 1/2, 1$) for $p = 0, \pm 1$.

3. Theoretical Methods of Reducing the Growth Rates

The maximum rate of growth can be decreased by quite a few methods, such as

(a) attenuating $\rho(k)$ at large $k\,\Delta x$ (easy and economical);

(b) use of higher-order weighting of particles and forces (each particle, expensive);

(c) use of NI interlacing grids in one time step, dropping $|\,p\,| = 1, 2, \ldots, \mathrm{NI} - 1$ aliases (inexpensive for NI = 2);

(d) combinations of the above;

(e) broader particles, obtained by use of particles nominally $M\,\Delta x$ wide (expensive).

The results of these methods will now be summarized.

Attenuating $\rho(k)$ where $\omega_i(k)$ is large (and objectionable) simply means putting in a smoothing factor SM(k) in the Poisson solver (a no-cost solution). SM(k) will have a low-pass characteristic, saving the desired physics (say, for $0 \leqslant k\,\Delta x \leqslant 1$) and dropping the rest ($k\,\Delta x = 1$ to π). Because smoothing is common and used to obviate other effects (such as nonlinear second harmonic feedback of $k\,\Delta x = 2\pi/3$, i.e., this $k\,\Delta x$ doubles due to nonlinear phenomena to $4\pi/3$, then aliases back to $2\pi/3$), this step is highly recommended. The approximate result is to decrease $\omega_i(k)$ to $\mathrm{SM}(k)\,\omega_{\mathrm{imag}}(k)$; this is an inexact statement (as the dispersion relation is more complicated) but sufficient for a first estimate.

Quadratic weighting, use of $r = 3$ in $S(k)$, Eq. (14), reduces the maximum growth rate to about

$$\omega_i \simeq 0.1\omega_p \qquad \text{at} \qquad k\,\Delta x \simeq 4\pi/5. \tag{17}$$

Interlacing, using two grids per time step (NI = 2), simply drops out the $p = \pm 1$ aliases but leaves growth between $p = 0$ and $p = 2$ harmonics, with maximum growth rate

$$\omega_i \simeq 0.05\omega_p \qquad \text{at} \qquad k\,\Delta x \sim 3\pi/4, \tag{18}$$

which is the same $(\omega_i)_{\max}$ as shown in Fig. 3 for $p = 2$ interaction. This result was also shown (at $k\,\Delta x = \pi/2$) by Chen *et al.* [2] in their Fig. 2, for $B = 0.12$.

With quadratic weighting and one interlace (NI = 2) the maximum growth rate is

$$\omega_i \simeq 0.01\omega_p \qquad \text{at} \qquad k\,\Delta x \simeq 3\pi/4 \tag{19}$$

All of the above refer to momentum-conserving programs

For energy-conserving programs, the dispersion relation Eq. (2) need have only the modification given by Eq. (13). Langdon [1] noted that such programs would have a threshold in B; he surmised stability for $B > 1/2\pi$. We found that there was stability for

$$B \geqslant 1/\pi. \tag{20}$$

We found growths, in the fundamental zone, of

$$(\omega_i)_{\max} \simeq 0.2\omega_p \text{ to } 0.3\omega_p \tag{21}$$

for $B = 1/4\pi$ and $1/2\pi$; no growth was found for $B = 1/\pi$, 1, 2, 3, and 4 using $p = 0, \pm 1, \pm 2$. [That is, we did not establish the sharpness of the inequality in Eq. (20).]

The last modification tried was the use of particles nominally (no grid) $M\,\Delta x$ wide; such particles are seen by the grid in linear weighting as trapezoidal in shape, with base width of $(M + 1)\,\Delta x$ and top width of $(M - 1)\,\Delta x$. For solving Eq. (2), we need the transform of this trapezoidal shape, which is

$$S(k) = \left[\frac{\sin(k\,\Delta x/2)}{(k\,\Delta x/2)}\right]\left[\frac{\sin(Mk\,\Delta x/2)}{(Mk\,\Delta x/2)}\right], \qquad M = 1, 2, 3, \ldots . \tag{22}$$

The first zero of $S(k)$ is at $k\,\Delta x = 2\pi/M$, which falls in the fundamental zone for $M \geqslant 2$, implying reduced alias coupling for $M \geqslant 2$. Growth rates are found as follows:

Particle width, M	$(\omega_i)_{\max}/\omega_p$	$k\,\Delta x$ at $(\omega_i)_{\max}$
1	0.205	2.4
2	0.103	1.75
3	0.056	1.2
4	0.036	0.9
8	0.012	0.45

Clearly $(\omega_i)_{\max}$ decreased (like $1/M$), but so does the region where interesting physics might be done [say, for $0 < k\,\Delta x < k\,\Delta x$ at $(\omega_i)_{\max}$]. The broader particles, while reducing the alias coupling, also reduce the resolution, demanding an increase in the number of grid points if the resolution is to be regained. Worse yet, the additional particle and force weighting (for $M \geqslant 2$ relative to the common $M = 1$, CIC or PIC) is expensive in computation time. Finally, as kindly pointed out to us by Langdon, our $S(k)$, which appears as $S^2(k_p)$ in Eq. (2), can be factored as

$$S^2(k_p) = \underbrace{\left[\frac{\sin(k_p\,\Delta x/2)}{(k_p\,\Delta x/2)}\right]^4}_{S^2(k_p)_{M=1}} \underbrace{\left[\frac{\sin(Mk_p\,\Delta x/2)}{M\sin(k_p\,\Delta x/2)}\right]^2}_{\substack{\text{periodic in } k_p\,\Delta x, \\ \text{hence independent} \\ \text{of } p}} \tag{23}$$

such that the last factor can be taken outside the sum over p. That is, the whole effect of particle weighting ($M = 1, 2, 4, 8$, whatever) can be obtained in simulation by using a smoothing factor, which is the second factor in Eq. (23), at no cost over $M = 1$. The crowning insult is that this smoothing factor is rather poor (too much attenuation at small $k\,\Delta x$, where the physics is to be kept). A better choice is use of a rounded step-function smoothing with no damage to physics at small $k\,\Delta x$.

The choice of smoothing, weighting, and, or interlacing for diminution of ω_i is up to the user.

4. Simulation Results for Initially Cold Beam

Previous authors [1–4] have shown clearly that the instability exists, that it grows at about the calculated rate, and that the wavelengths observed in the aliases (in the particle phase-space plots, for $k\,\Delta x > \pi$) are at the proper values. However, they worked at $B \lesssim 0.12$, the slow-beam regime, where (we will see) stability or quiescence comes in only when the beam is heated to $v_t \gtrsim v_0$ (not a very distinct beam). Our results were obtained out to $B > 1$, where stability occurs with $v_t \ll v_0$. We present a verification of growth rates, the saturation or change-of-state, and stability criteria. The results presented are for a momentum-conserving program, with the three and two point finite-difference operators implied by Eqs. (11) and (12). Simulations using energy-conserving programs were given by Langdon [3] for his parameters, where the prime result was loss of the drift motion.

In all runs there were NP = 6400 particles of one sign and an immobile neutralizing background. Other units (arbitrarily chosen) were $q/m = 1$, $\omega_p = 1/2\pi$, $\Delta t = 2\pi/10$

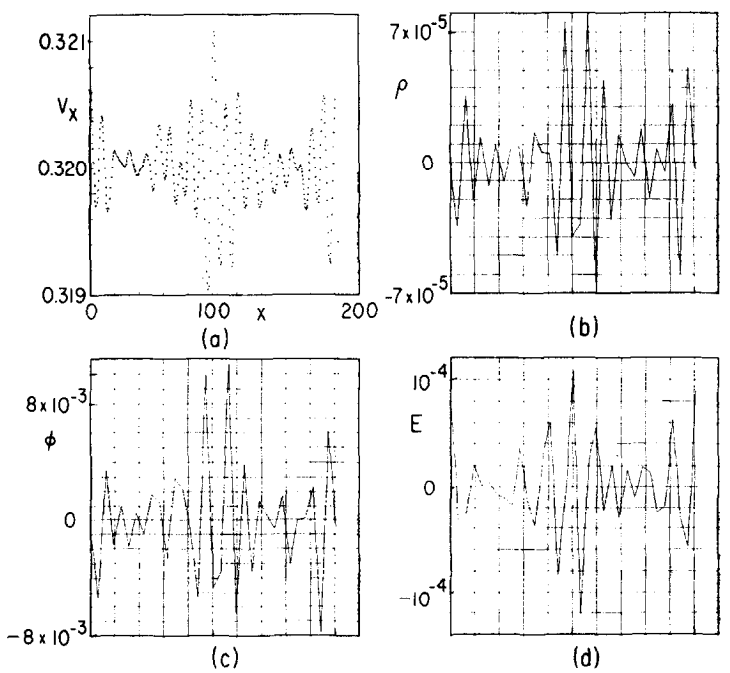

FIG. 6. Snapshots at $\omega_p t \simeq 25$ of (a) particle v_x versus x showing strong alias structure, at wavelengths shorter than two cells (19 or 20 peaks in 32 cells) and of (b)–(d) grid-measured charge density ρ, potential ϕ, electric field E, showing 11, 12, or 13 peaks. Mode 20 aliases to 12; mode 19 aliases to 13, as seen. $B = 0.32$, $\omega_p/\omega_p \simeq 2$.

(so $\omega_p \Delta t = 0.1$), $k_{\min} = 1/32$ (so $L = 2\pi \times 32 = 201.06$); the number of cells, NG, was 32 (used in most runs), so $\omega_p \Delta x = 1$; hence, in these units $B = v_0$, $\lambda_D/\Delta x = v_t$. There was no smoothing; SM(k) = 1 for all k.

The behavior for $B = 0.32$ displays features for most other values of B and was shown earlier in analysis. Hence, this will be explored in some detail.

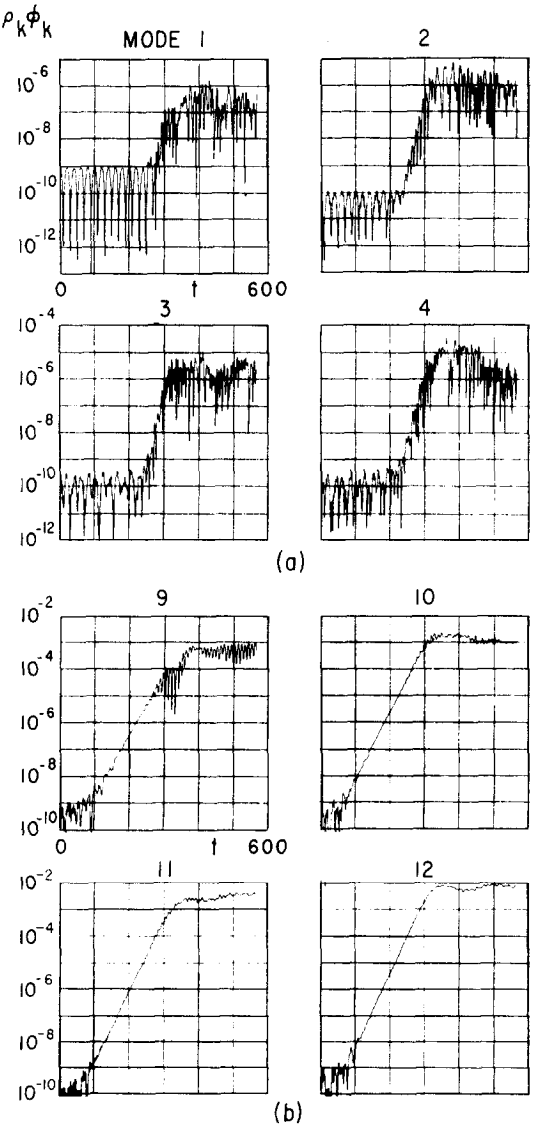

FIG. 7. Electrostatic energy versus time for (a) modes 1, 2, 3, 4, which have almost no linear growth rate, and for (b) modes 9, 10, 11, 12, which have linear growth rates $\omega_i/\omega_p \simeq 0.2$; $B = 0.32$, $\omega_g/\omega_p = 2$.

The particles were given a random displacement of $\delta x = 0.01$ either side of uniform spacing (or $1/32 = 0.0325$); there was no initial velocity perturbation. Mode 8 (out of 16) was clearly seen in the phase space (v_x, x) plot at $t = \Delta t/2$. Well into the run (after about four plasma cycles, $\omega_p t \simeq 25$, $t \simeq 150$) the effects of the aliasing are very clearly seen, as displayed in Fig. 6: In Fig. 6a v_x versus x shows 19 or 20 distinct peaks (i.e., modes 19 and 20 would be relatively large if a continuous Fourier analysis were made); in Fig. 6b charge density ρ versus x, there are 13 distinct peaks; in Fig. 6c potential ϕ versus x, there are 12 distinct peaks; and in Fig. 6d electric field E versus x, there are 11 distinct peaks. With NG = 32 cells, 16 modes can be found by finite Fourier analysis (as used here in ρ, ϕ, and E); the modes seen in $v_x - x$ plots beyond mode 16 are aliased into the fundamental zone about mode 16. That is, mode 20 in $v_x - x$ is read as mode $16 - (20 - 16) = 12$; mode 19, as $16 - (19 - 16) = 13$, as is clearly the situation here.

The individual modes were observed to grow as shown in the Fig. 7 plots of $\rho_k \phi_k^*$ for modes 1 through 4 and 9 through 12. In Fig. 7a for the long wavelength modes, the early growth observed is very small, with plasma oscillations in mode 1 of period

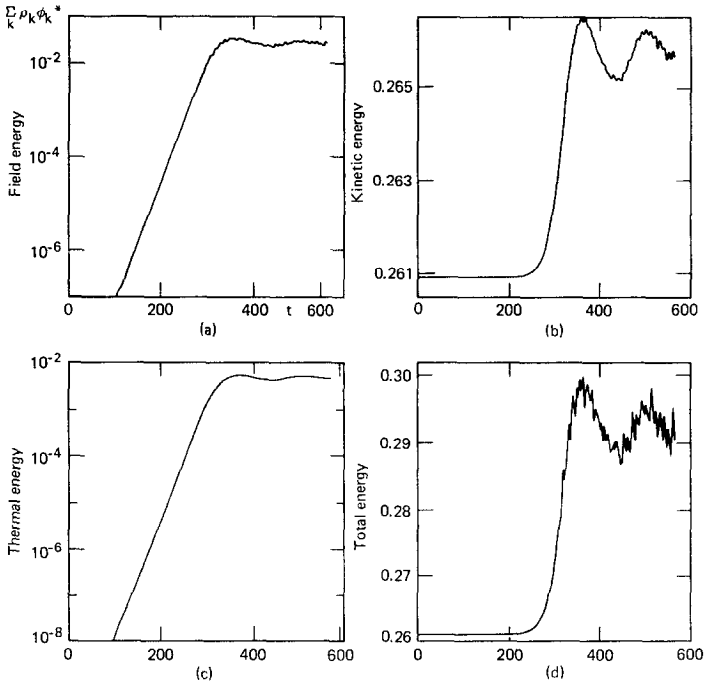

FIG. 8. System energies versus time, for $B = 0.32$: (a) shows total electrostatic energy growth to saturation, about 11 % of the initial kinetic energy, (b) shows total kinetic energy $\frac{1}{2}mv^2$, increasing by a little over 2 % of all particles, (c) shows thermal energy, $\frac{1}{2}m(\overline{v^2} - \bar{v}^2)$ of all particles increasing to saturation, about 2 % of the kinetic energy, and (d) shows the total system energy, which grows by about 15 %, a real error; however, after saturation with the beam now slightly warm, there is no further growth and the total energy fluctuates roughly $\simeq$0.7 %, typical of stable programs.

$\tau = 40$ as against $\tau_p = (2\pi)^2 \simeq 39.5$ (not quite right either, as noted in the $\omega - k$ plots of Fig. 4, but close). In Fig. 7b the faster growing modes take off early, growing about 10^7; the lack of oscillatory behavior is due to display of $\rho_k \phi_k^*$ for a traveling wave, which drops the ω_{real} part. The linear growth rates for modes 8 through 15 were measured (ranging from ω_i/ω_p of 0.145 to 0.208), falling almost exactly on top of the prediction of Fig. 4. The later-time growths of modes 1 through 4 is taken to be due to nonlinear interactions, occurring beyond $t = 250$ when modes 9 through 12 have reached large amplitudes and are probably beating among themselves, physically.

All of the system energies grow due to the instability, as shown in Fig. 8. In Fig. 8a the field energy grows at a rate close to that of the fastest growing mode ($\omega_i/\omega_p \simeq 0.188$) to a level of about 11 % of the initial kinetic energy. In Fig. 8b the kinetic energy grows similarly. In Fig. 8c the thermal energy (obtained from $\overline{v^2} - \bar{v}^2$) grows and saturates; a thermal velocity is defined from the saturation value as

$$\frac{v_t}{v_0} \equiv \left(\frac{\text{thermal energy at saturation}}{\text{kinetic energy at } t = 0}\right)^{1/2}.$$

While we have some measures of the velocity distribution, we cannot demonstrate that we observe $f(v) \sim \exp(-(v - v_0)^2/2\, v_t^2)$. In Fig. 8d the total energy is seen to grow by about 15 %; that is, energy conservation is lost due to the nonphysical instability. The fluctuations in total energy after saturation are about ± 0.7 %, which would be acceptable "conservation" for most runs, especially when the potential energy is as large as it is here.

The *saturation behavior* signals an end to rapid self-heating due to the gridding; the initially cold beam has acquired a spread in velocities, the particles are now crossing, and total energy is now well conserved.

5. Simulation Results for an Initially Warm Beam

The obvious question is why not add an initial velocity spread to the beam and see whether there is less growth or stability? This was done. An initial random (Gaussian) velocity modulation was added at $t = 0$ starting with $v_{\text{thermal}}(t = 0) < v_t$ (at saturation for an initially cold beam). The instability still occurred; the saturation energies remained the same, simply occurring earlier in time, as shown in Fig. 9. Next, starting out with $v_t(t = 0) = v_t(\text{saturation})$, little growth occurs (about $10^{1.3}$ in mode 12 at $k\,\Delta x = 3\pi/4$); there is an initial rapid rise in field energy (in a time of about τ_p) to a value 10 times smaller than for $v_t(t = 0) = 0$, doubling later as mode 12 saturates. The thermal energy is essentially flat in time. The total energy rises about 1 part in 300. Finally starting with $v_t(t = 0) = 2v_t(\text{saturation})$, the field energy immediately rises to a value 100 times smaller than for $v_t(t = 0) = 0$ and stays there, the thermal energy maintains its initial value, and the total energy fluctuates about 1 part in 500. There are no growing modes.

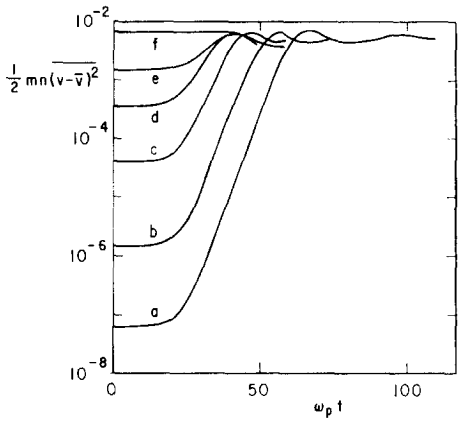

FIG. 9. Thermal energy of all particles versus time, with various initial thermal velocities (about v_0) measured in terms of $v_t/\omega_p \Delta x$: $a = 1.59 \times 10^{-4}$; $b = 7.95 \times 10^{-4}$; $c = 3.98 \times 10^{-3}$; $d = 1.19 \times 10^{-2}$; $e = 2.39 \times 10^{-2}$; $f = 5 \times 10^{-2}$. The mean value after saturation appears as $0.047 \simeq 0.001$. All initial values at or above this value remain at their initial values.

6. STABILITY CRITERION

The saturation value of v_t for an initially cold beam is shown in Fig. 10 for eight values of B, $0.08 \leqslant B \leqslant 1.28$. The curve drawn through these points is taken to divide the *stable* and *unstable* regions on the basis of the simulations of the preceding section; that is, for $v_t(t = 0)$ below the curve, v_t grew to the curve and stopped; for $v_t(t = 0)$ above the curve, v_t did not grow.

There appear to be two regions; the first occurs for

$$B \leqslant 1/(2\pi) \qquad \text{where} \qquad \omega_{\text{grid}} \lesssim \omega_p \text{ or } v_0/\Delta x < f_p$$

and the second for

$$B \gtrsim 1/(2\pi) \qquad \text{where} \qquad \omega_{\text{grid}} \gtrsim \omega_p \text{ or } v_0/\Delta x > f_p .$$

At $B = 0.3$, $(v_t/\omega_p \Delta x) \gtrsim 0.046$ or $v_t \gtrsim 0.138 v_0$ is stable. At $B = 1.28$, stability requires $v_t \gtrsim 0.036 v_0$. That is, as B increases, the thermal spread about v_0 required for stability decreases.

The simulator has a choice: one may start with a cold beam and let the nonphysical growth mechanism provide growth of v_t to a saturated value or one may start with a warm beam, $v_t > v_t$ saturated, see no growth and, as noted earlier, have much smaller electric field energy (quieter).

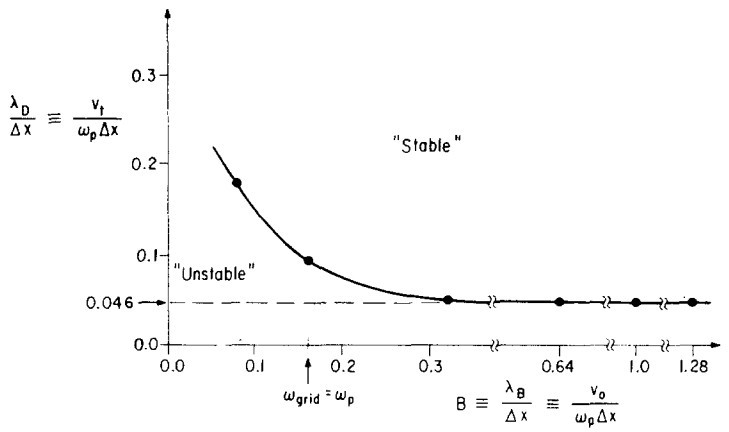

FIG. 10. Experimental determination of the thermal spread needed for stability of a beam in a (mathematically) gridded periodic system, using a momentum-conserving program.

7. MECHANISM OF SATURATION

The question is why does saturation and stabilization occur at $v_t/\omega_p \Delta x \simeq 0.046$ for all $B = v_0/\omega_p \Delta x \gtrsim 0.3$. An answer has been provided by Albritton and Nevins [7] in terms of saturation by particle trapping. Their argument is now given.

It is convenient to define a frequency,

$$\Omega \equiv \omega - k_1 v_0 .$$

Strong coupling between the $p = 1$ alias mode and the beam will occur when $\omega/k_1 \simeq v_0$, i.e., when Ω is small. Hence, we consider the limit $\Omega/\omega_p \ll 1$. In addition, we restrict our attention to small values of k, such that $k/k_g \ll 1$, and assume that $k_g v_0/\omega_p \gg 1$. The leading terms in the dispersion relation (for $p = 0, 1$ only) are then

$$\Omega^2/\omega_p{}^2 = -[\zeta^3/(1 - \zeta)^3](1 - \pi^2\zeta^2),$$

where

$$\zeta = k/k_g .$$

Hence, Ω is purely imaginary for small, positive ζ. The maximum growth rate is determined by choosing ζ to maximize the absolute value of Ω^2. We find

$$\gamma_{max} = 0.2\omega_p$$

at

$$k/k_g = 0.4,$$

which is the same as the roots given earlier, Eq. (15).

In this limit (i.e., $k_y v_0/\omega_p \gg 1$) saturation occurs due to the trapping of beam particles in the electric field of the *alias* wave. This trapping occurs when

$$k_1 \delta_1 = 1,$$

where δ_1 is the Lagrangian displacement of the beam particles due to the presence of the alias wave.

The velocity spread of the beam, v_t, can be estimated from the Lagrangian displacement by

$$v_t = | \dot{\delta} | \simeq | \Omega \delta_1 |,$$

where in writing the second equality we have used the fact that Ω is the frequency of the alias wave in the reference frame of the beam. Since trapping occurs when $k_1 \delta_1 = 1$, it follows that the beam spread at saturation is estimated from

$$v_t = | \Omega / k_1 |.$$

Substituting the appropriate values for the fastest growing mode gives

$$(v_t)_{\text{saturation}} \approx 0.05 \omega_p \Delta x.$$

Finally, using the Debye length of the beam as $\lambda_D = v_t \omega_p$, this result may be written as

$$\lambda_D / \Delta x \simeq 0.05.$$

This value is in excellent agreement with the simulation results. In addition, Fig. 6 shows the bunching of the beam in $v_x - x$ space with a spacing equal to the wavelength of the $p = 1$ alias; at later time, these bunches form into vortices as is common in trapping.

Hence, we conclude that this simple trapping model accurately describes the saturation of the grid–alias instability in the limit of a fast cold beam.

8. Self-Heating of a Maxwellian at Small $\lambda_D/\Delta x$

A Maxwellian distribution is also nonphysically unstable for momentum conserving codes, especially for small values of $\lambda_D/\Delta x$. The small amplitude growth was predicted by Langdon [1] and observed by Langdon [1], Okuda [4], and Chen *et al.* [2]. However, the long term evolution was not found; this we have done. A Maxwellian was loaded with $\lambda_D/\Delta x = 0.1$, which is nonphysically unstable. The simulation was allowed to run for a very long time ($\omega_p T \sim$ few 1000), during which v_t increased slowly and appeared to approach $\lambda_D/\Delta x \simeq 0.3$ asymptotically, where the small amplitude growth rate becomes quite small. Hence, the Maxwellian heats up to a new state, just as does the cold beam.

9. Effect of Aliasing on the Physical Two-Stream Instability

Many two-stream and beam–plasma interactions have been simulated over the past two decades, with no obvious reference, to our knowledge, to the effects of aliasing. There may have been unexplained anomalous effects that were small and ignorable or perhaps the simulators chose parameters to minimize aliasing effects. In any case, it seemed wise to us to solve the dispersion relation with aliases for a range of parameters in order to display the nonphysical effects of the aliases on the physical two-stream instability.

First, we show the $p = 0$ solutions, for which there is no aliasing, in Fig. 11. However, the grid effects in the fundamental zone remain (K and κ in place of k), showing up as $\omega_{\text{imag}}/(\omega_p)_{\max}$ dropping off from 0.5 (no grid) as it occurs at larger and larger $k\,\Delta x$.

Second, we show the $p = 0, \pm 1$ solutions, in Fig. 12. Including $p = \pm 2, \pm 3$, etc., presumably would add more (but slower) growing nonphysical roots, judging by the single-beam results. These aliases were omitted in order to avoid even more complicated diagrams.

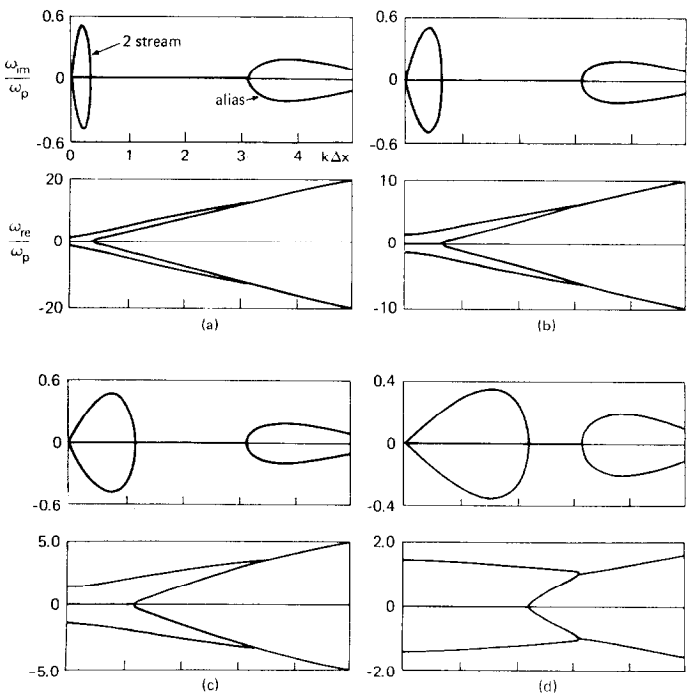

FIG. 11. Dispersion diagrams, ω/ω_p versus $k\Delta x$ for $p = 0$ (no aliasing) for two opposing beams, showing the physical two-stream instability. The fundamental-zone grid effects remain; (a)–(d) are for ($B = v_0/\omega_p\Delta x = 4.0,\ 2.0,\ 1.0,\ 1/\pi \simeq 0.318$), with $[\omega_{\text{imag}}/(\omega_p)_{\max} = 0.4967,\ 0.4890,\ 0.4631,\ 0.3446]$ dropping off as this maximum occurs at larger $k\Delta x$ ($= 0.22, 0.42, 0.76, 1.52$). Also, $(\omega_p)_{\text{effective}}$ is seen to vanish as $k\Delta x \to \pi$.

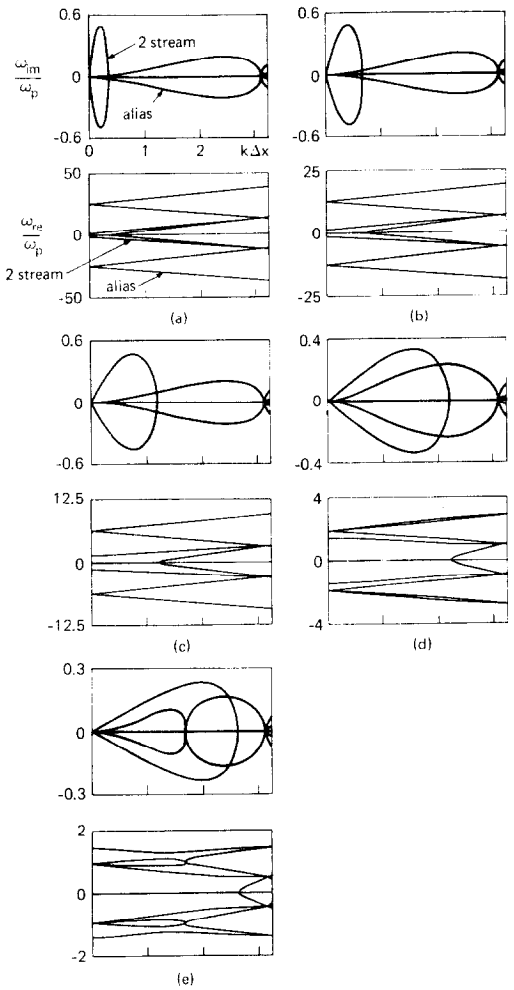

FIG. 12. Same as Fig. 11, with $p = 0$, but also with $p = \pm 1$ aliases. (a)–(e) are for ($B = 4.0$, 2.0, 1.0, 0.3, 0.15), with maximum two-stream growth rates much as before.

For $B \gtrsim 1$, for k in the two-stream unstable range, the two-stream physical growth far exceeds that due to aliasing; for larger k, all B, there is only the alias growth, with a maximum of about two-fifths that of the two-stream maximum growth.

For B decreasing below 1.0, $\partial\omega_r/\partial k$ of the physical two-stream branch changes sign. For $B < 1/[(2)^{1/2}\pi]^{-1} = 0.224$, ω_g decreases below $(2)^{1/2}\,\omega_p$, which is the $k = 0$ intercept of the two-stream ω_{real}. At this small B, ω_{real} of the two-stream has switched above that of the alias instability and two branches to ω_{imag} have come in, obscuring the physical behavior.

There also is a physical multistream instability, pointed out long ago by Dawson [8] and simulated more recently by Gitomer and Adam [9]. In their simulations the

initial velocity distribution function was a Maxwellian envelope made up of many cold beams. They observed the physical multistream instability growth (good check between linear theory and simulation), which then saturated at a level of (electric field energy) $\ll$ (kinetic energy), roughly that expected of a fully random Maxwellian. Their total energy remained nearly constant (within 0.1 %), a trademark of physical behavior. The saturation, from seeing vortices in phase-space plots, appears to be by particle trapping. The point is that the growth seen here, while due to a trick used in simulation (many beams to represent a Maxwellian), is physical, predictable from theory for $\Delta x \to 0$, $\Delta t \to 0$, and is *not* due to the spatial or temporal grid.

10. Discussion

The cold beam instability caused by the numerical grid is found to be self-quenching, due to self-heating and particle trapping of the beam. For reasonable parameters, $\lambda_B \equiv v_0/\omega_p \Delta x \gtrsim 1$, the quench and return to stability occurs for $v_t \ll v_0$; this slight heating is an almost ignorable change for many simulations. Hence, while the instability has a very large growth rate, the net effect of slight self-heating may be negligible. However, for some parameters, such as $v_0/\omega_p \Delta x \lesssim 0.3$, $k \Delta x \gtrsim \pi/2$, the nonphysical effects could swamp the physical problem being studied, so that care in design is still demanded. These comments apply only to momentum-conserving programs, such as CIC and PIC.

Acknowledgments

We gratefully acknowledge the continued suggestions and interest of A. B. Langdon, beyond the specific references made in the text, and the use of unpublished material on the saturation mechanism by J. Albritton and W. M. Nevins.

References

1. A. B. Langdon, *J. Computational Phys.* **6** (1970), 247; in *Proceedings of the 4th Conference on Numerical Simulation of Plasmas, Naval Research Laboratory*, 1970, p. 467.
2. L. Chen, A. B. Langdon, and C. K. Birdsall, *J. Computational Phys.* **14** (1974), 200.
3. A. B. Langdon, *J. Computational Phys.* **12** (1973), 247. See Figs. 1 and 2.
4. H. Okuda, *J. Computational Phys.* **10** (1972), 475.
5. A. B. Langdon, *Phys. Fluids* **22** (1979), 163.
6. C. K. Birdsall, N. Maron, and G. Smith, presented at the 7th Conference on Numerical Simulation of Plasmas, Courant Inst., New York University, 1975.
7. J. Albritton and W. M. Nevins, unpublished report.
8. J. M. Dawson, *Phys. Rev.* **118** (1960), 381.
9. S. J. Gitomer and J. C. Adam, *Phys. Fluids* **19** (1976), 719.